Chemical Science

EDGE ARTICLE

Check for updates

All publication charges for this article have been paid for by the Royal Society of Chemistry

Dynamic satellite–parent liposome networks for quantitative microreactions†

Jia-Qi Tian[a] and Nan-Nan Deng [ID] *[ab]

The hierarchical assembly of liposomes into interconnected networks forms the basis for creating rudimentary artificial multicellular systems. Each vesicle performs specialized functions both temporally and spatially, replicating the complexity of living tissues. Controlling the size and number of liposomes in artificial multicellular systems and their dynamic interactions are necessary for quantitative bioprocesses but remain challenging. Here, we develop a satellite–parent liposome network—a central parent liposome surrounded by smaller satellite liposomes. This structure spontaneously forms during the dewetting transition of microfluidically prepared complex double emulsions. Intriguingly, the adhesion strength between the satellites and the parent liposome can be tuned using environmental stimuli. The varying numbers of satellite liposomes provide an excellent platform for studying quantitative microreactions. To illustrate, we first explore the differences in molecular affinity between parent and satellite liposomes to achieve directional molecular transfer against concentration gradients. Then, we mimic quantitative signal transfer by performing enzymatic reactions, supplying substrates from different numbers of satellites to the parent liposomes. After the reaction, the satellites can be separated from the parent liposome on demand upon osmotic stimuli. This work showcases an exceptional dynamic liposome network that will facilitate the mimicry of the complexity of multicellular systems *in vitro*.

Introduction

Modular compartmentalization of chemical and biological processes is one of the vital organizational features in living systems.[1–3] Cells perform the functions of life in separate compartments that communicate,[4] cooperate,[5] and sense environmental changes,[6] thereby generating emergent properties essential for life. Mimicking this biological compartmentalization at micrometre scales holds significant promise for technological development across myriad fields, including multistep micro-/nano-reactors, synergistic drug delivery systems, and synthetic cell networks.[7–13]

Liposomes, synthetic compartments containing bilayer membranes, have been widely utilized as artificial cells due to their ability to encapsulate and protect active substances, and thus have been used as microcompartments to mimic fundamental aspects of natural cells,[12–14] such as gene transcription,[15,16] protein synthesis,[17,18] molecular transport,[19] oscillation,[20,21] cell division[22,23] and energy production and storage.[17,24] Furthermore, the hierarchical assembly of liposomes into interconnected networks forms the basis for

creating rudimentary artificial multicellular systems, in which each vesicle performs specialized functions both temporally and spatially, replicating the complexity of living tissues. Activities such as cascade enzymatic reactions,[25–27] thermoresponsive volume changes,[28,29] predatory behaviour,[30] signal transmission[31,32] and power generation[33,34] have already been demonstrated. Molecular transfer between each microcompartment is essential in driving these collective behaviors. To facilitate transmembrane transport of molecules, membrane proteins like α-hemolysin are often inserted into the bilayer membranes, forming nanopores that allow free diffusion driven by concentration gradients of cargoes.[35–38] However, this free diffusion typically results in a homogeneous distribution of the target molecules within the sub-microcompartments,[36,37] leading to relatively low transport efficiency. Moreover, current research on tissue-like multicompartment systems has primarily focused on qualitatively demonstrating the proof-of-concept of coupled cascade reactions among their subunits. Controlling the size and number of liposomes in artificial multicellular systems and their dynamic interaction necessary for more complex and quantitative microreactions remains challenging.

Here, we report an interesting satellite–parent liposome network—a central parent liposome surrounded by smaller satellite liposomes. This structure spontaneously forms during the dewetting transition of microfluidically prepared complex double emulsions, where the inner cores can be precisely

[a]Shanghai Jiao Tong University, School of Chemistry and Chemical Engineering, Shanghai 200240, China. E-mail: n.deng@sjtu.edu.cn

[b]Shanghai Jiao Tong University Sichuan Research Institute, Chengdu, Sichuan, 610213, China

† Electronic supplementary information (ESI) available. See DOI: https://doi.org/10.1039/d4sc04925j

controlled. Intriguingly, the adhesion strength between the satellites and the parent liposome can be tuned using environmental stimuli, such as osmotic pressure. We demonstrate that the liposome clusters can function as chemical reaction networks, with different reactants loaded into separate compartments. The varying numbers of satellite liposomes provide an excellent platform for studying quantitative microreactions. To illustrate, we first explore the differences in molecular affinity between parent and satellite liposomes to achieve directional molecular transfer against concentration gradients. Then, we mimic quantitative signal transfer by performing enzymatic reactions, supplying substrates from different numbers of satellites to the parent liposomes. After the reactions are complete, the satellites can be separated from the parent liposome on demand using osmotic stimuli. This work showcases an exceptional dynamic liposome network, facilitating the mimicry of the complexity of multicellular systems *in vitro*.

Results and discussion

Microfluidic construction of satellite–parent liposome networks

To construct satellite–parent liposome networks, we used a strategy of dewetting transition of water-in-oil-in-water (W/O/W).[15] A two-stage microcapillary-based microfluidic device that consists of two droplet generators at the first stage was

employed to prepare two different water-in-oil (W/O) droplets which were subsequently paired and encapsulated into W/O/W droplets at the second stage of the device, thereby forming complex W/O/W droplets with different inner droplets (W1 and W1′) (Fig. 1a and S1b†). The key to successful fabrication of satellite–parent liposomes is to control the size ratios of the W1/O to W1′/O droplets. The large one was identified as the parent, and the smaller ones were the satellites. The W1 and W1′ phases were aqueous solutions of 2% (w/v) PVA and 8% (w/v) PEG labelled with fluorescein isothiocyanate (FITC)-dextran and tetramethyl rhodamine (TRITC)-dextran, respectively. The O and W2 phases were respectively mixtures of chloroform and hexane (36 : 64, v/v) with 5 mg mL^{-1} DOPC, and aqueous solutions of 10% (w/v) PVA and 1.5% (w/v) Pluronic F-68. In the W/O/W templates, droplet interface bilayers (DIB) were first formed when the interior W1/O and W1′/O droplets were brought in contact. Then the DIB-connected interior droplet networks underwent a dewetting transition to form liposome networks *via* the spontaneous removal of the oil phases (Fig. 1b). The whole processes were driven by interfacial energy. By simply varying the flow rates, we prepared satellite–parent liposome networks with 1–8 and more satellite compartments (Fig. 1c and
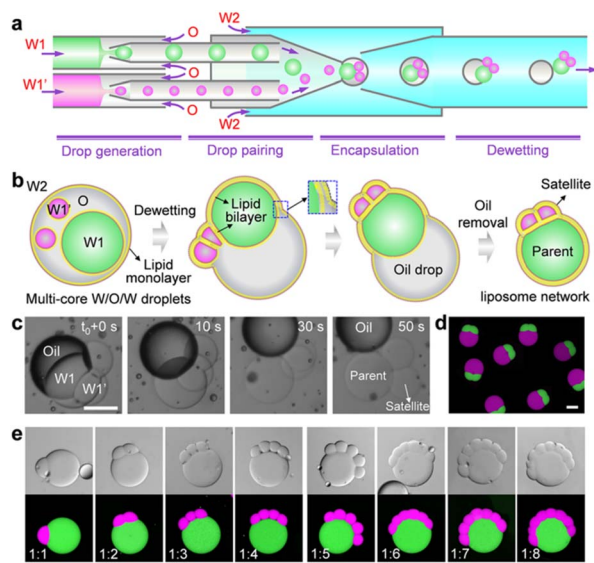

Fig. 1 Microfluidic construction of satellite–parent liposome networks. (a) Scheme of the preparation of complex W/O/W double emulsions with two types of inner cores in a microcapillary-based microfluidic device. (b and c) Scheme and optical images of assembly of satellite–parent liposome networks from dewetting of complex W/O/W templates. (d) Overview confocal image of satellite–parent liposomes. (e) CLSM images of as-prepared satellite–parent liposomes with controlled satellite compartments (from 1 to 8 satellites). The parent liposomes were labelled by FITC-dextran (green) and the satellites were dyed by TRITC-dextran (magenta) stain. Scale bar, 100 μm.
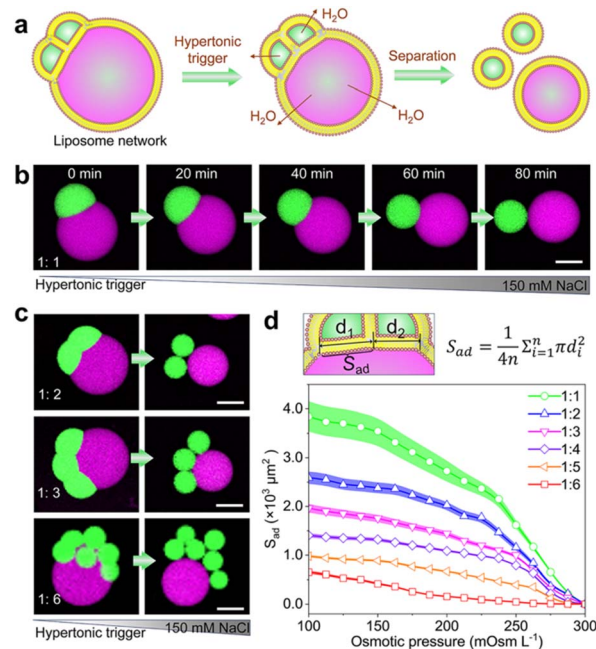

Fig. 2 Osmosis-induced dynamic adhesion in satellite–parent liposomes. (a and b) Schematics (a) and CLSM images (b) of the shrinking and separating processes of satellite–parent liposomes in response to hypertonic shock (150 mM NaCl) (green, FITC-dextran stain; magenta, TRITC-dextran stain). The initial interior and exterior osmotic pressures of satellite–parent liposome networks were about 100 mOsm L^{-1}. (c) CLSM images showing the separation of satellite–parent liposomes (satellites : parent = 1 : 2, 1 : 3 and 1 : 6) in response to 150 mM NaCl. (d) Equation for calculating adsorption area and plots showing the variations of adhesion areas between the satellite liposomes and the parent liposomes during the shrinking and separating processes. S_{ad} is the adhesion areas between the satellite liposomes and the parent liposomes. d is the diameter of the adsorption surface circle. n is the number of the satellite liposomes. Scale bars, 100 μm.

$$S_{ad} = \frac{1}{4n}\Sigma_{i=1}^{n}\pi d_i^2$$

S2†). The key to successful fabrication of satellite–parent liposomes is to control the size ratios of the W1/O to W1′/O droplets. It requires a large W1/O droplet and several much smaller W1′/O droplets, and *vice versa*. When their sizes are comparable, they will form random liposome networks (Fig. S3†), instead of satellite–parent ones. Interestingly, the flow in the microchannels drags the "satellite" compartments into contact with each other (Fig. S4†). Furthermore, different types of satellite liposomes can also be created by adding more droplet generators at the first stage of the microfluidic device. For demonstration, satellite–parent liposome networks with two different types and numbers of satellites were successfully prepared (Fig. S5†). Similarly, when W1/O, W1′/O, W1″/O droplets sizes are comparable, they may form liposome networks with various configurations but not the satellite–parent manner (Fig. S6†).

Dynamic morphologies in satellite–parent liposome networks

Membrane dynamics and remodelling are the key features of biological membranes and dominate diverse cellular processes, such as cell division,[39] cell movements,[40] and cargo transport.[41] Next, we show that the satellite–parent liposome networks readily exhibit morphological dynamics of adhesion in response to environmental changes. As Fig. 2a shows, we used an osmotic shock to induce the separation of the satellites and the parent liposomes. When a hypertonic trigger (150 mM NaCl) was added into the satellite–parent liposome networks, the contact area between subunits was reduced gradually until complete separation (Fig. 2b). We attribute this dynamic process to the increase of surface-to-volume ratios of the sub-compartments due to the loss of internal water through the semipermeable lipid bilayers. The satellite–parent liposome networks deform and separate to minimize the energy associated with the line tension at the phase boundary.[42] Similarly, for the networks with more satellite liposomes, hypertonic osmosis resulted in the complete separation of the liposomal sub-compartments (Fig. 2c, S7 and S8†). The adhesion areas (S_{ad}) between the single satellite liposomes and the parent liposomes were calculated according to the morphological changes (Fig. 2d), representing the variations of the areas for mass transfer between the subunits. The adhesion area (S_{ad}) decreases over time until satellite liposomes are completely separated from the parent liposomes and dropped to 0 (Fig. 2d).

Directional and quantitative transport of molecular cargoes

The resultant satellite–parent liposomes and their membrane dynamics provide exceptional models for quantitative transmembrane transport of molecular cargoes. To demonstrate, we here used a membrane peptide melittin to create nanopores in
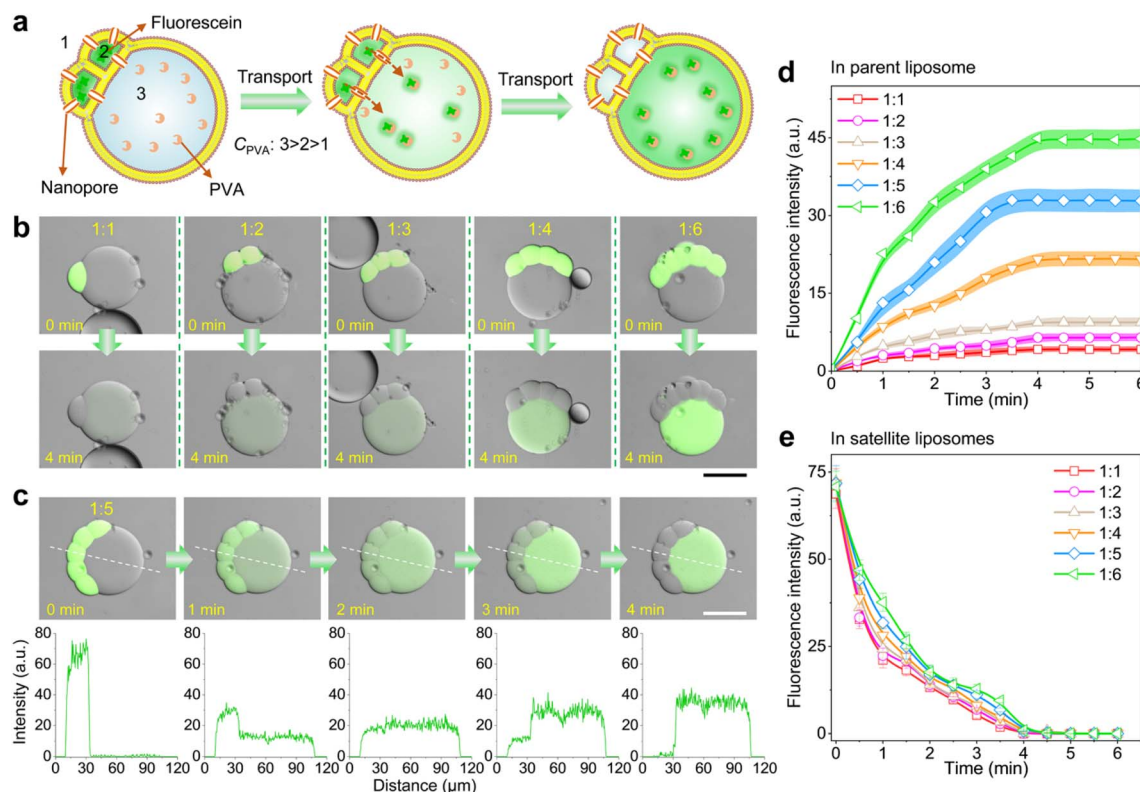

Fig. 3 Directional and quantitative transport of molecular cargoes from satellites to parent liposomes. (a–c) Schematics (a) and CLSM images (b and c) showing molecular binding affinity-directed transport of fluorescein from different number of satellite compartments (from 1 to 6) to the parent compartments. (c) showing the detailed process of the molecular transport and the relevant fluorescence intensity profiles in a 5-satellite–parent liposome. PVA concentrations are respectively 3% (w/v) in the satellite compartments (2), 5% (w/v) in the parent compartments (3) and 1% (w/v) in the outer phase (1). (d) and (e) Kinetics of fluorescent signals in the parent compartments (d) and those in the satellite compartments (e). Scale bars, 100 μm.

the bilayer membranes of the liposome networks, allowing for molecular transfer, and explored the differences of molecular binding affinity between cargoes and the different interiors of the satellite–parent liposomes to achieve the directional transport. Binding affinity describes the strength of the binding between a single biomolecule (such as protein or DNA) and its ligand/binding partner (such as drug or inhibitor), and is influenced by non-covalent intermolecular interactions like hydrogen bonding, electrostatic interactions, hydrophobic forces and van der Waals forces between the two molecules.[43,44] We chose fluorescein as a model molecule, as it is impermeable to the lipid bilayer, and has a higher binding affinity with PVA than that with PEG.[19] As Fig. 3a shows, we encapsulated fluorescein ($0.5\ \mu M\ L^{-1}$) and melittin monomers ($2\ \mu M$) into the satellite compartments, and meanwhile created a concentration gradient of PVA as $C_3 > C_2 > C_1$ across the bilayer membranes. After incubation, we observed that the mass transfer of fluorescein from the satellite compartments to the parent liposomes over time (Fig. 3b, c and S10†). The whole transport process took about 4 min. The fluorescence intensity of the parent compartments increased colligatively with the number of satellite compartments (Fig. 3d). The more satellites, the

higher fluorescent signals in the parents. Strikingly, the speed and efficiency of the molecular binding affinity-directed transport is much higher than that of free diffusion without PVA gradients (Fig. S11†). After equilibrium was reached, the residual fluorescein molecules in the satellites were undetectable under a confocal microscope (Fig. 3e), indicating that the transport even occurs against the concentration gradients. No leakage of fluorescein to the outer environment was detected (Fig. 3c), though the nanopores exist in the whole membranes of the satellites. Additionally, binding affinity-mediated directional transport mechanisms are widely applicable and have great potential to enhance the design and functionality of synthetic tissues. By utilizing the differential binding affinities of biomolecules such as protein–protein interactions, DNA binding, and ligand-receptor dynamics proteins, one can create highly specific and directional transport systems that replicate the efficiency and precision seen in natural systems.

Satellite–parent liposomes for quantitative micro-reactions

We finally demonstrate the satellite–parent liposome networks are promising platforms for quantitatively performing micro-
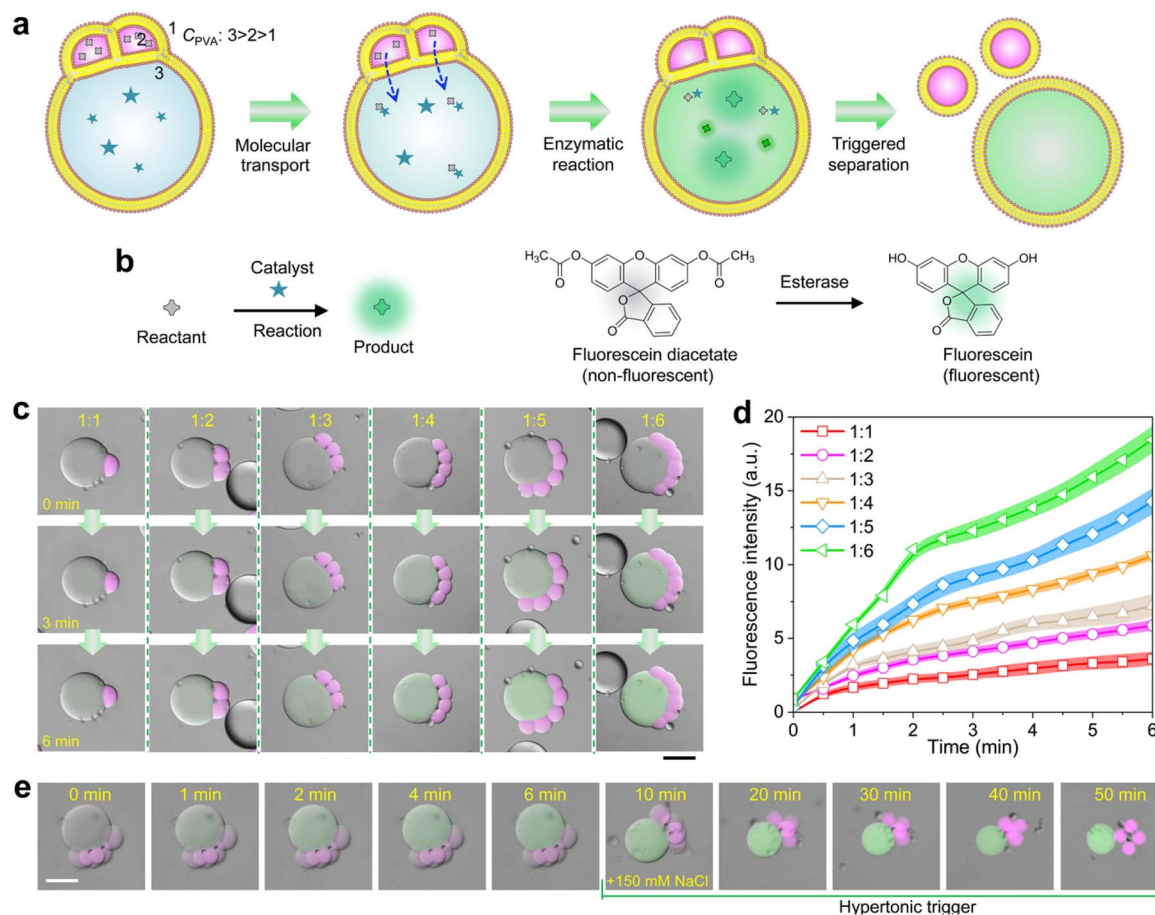

Fig. 4 Satellite–parent liposome networks for quantitative micro-reaction. (a–c) Schematics and confocal images showing non-fluorescent substrates (fluorescein diacetate) are transported from different numbers of satellites (1–6) to parent compartments. (b) showing the enzymatic degradation of the substrates to generate fluorescein (green). (d) Kinetics of fluorescent signals in the parent liposomes in (c). (e) CLSM images showing the reaction and detachment between satellites and their parent liposomes in a hypertonic trigger. Scale bars, 100 μm.

reactions. We encapsulated 5% (w/v) PVA and enzymes (esterase, 0.1 units per mL) into the parent compartments, and 3% (w/v) PVA and the substrates (fluorescein diacetate) into the satellite, respectively. The PVA concentration in the outer phase was 1% (w/v) which is lower than that in all the liposomes.

In this case, the substrates in satellite compartments were successfully transported into the parent liposomes, inducing the enzymatic degradation of the substrates to generate fluorescein in the parents (Fig. 4a–d and S12†). As Fig. 4c shows, the fluorescence intensity of fluorescein inside the parent compartments increases colligatively when the number of satellite compartments increase from 1 to 6 (Fig. 4d). After the reaction was completed, the detachment between the satellite compartments from the parent was performed by applying a hypertonic trigger, finally forming independent liposomes (Fig. 4e). Notably, by incorporating magnetic Fe_3O_4 nanoparticles into the satellite compartments, we can effectively collect either parent or satellite liposomes after the reaction and separation process. The satellite liposomes can be directed to the target site using a magnet, while the parent liposomes remain stationary (Fig. S13 and S14†). This method allows for the selective collection of different products post-reaction.

Conclusions

Dynamic satellite–parent liposome networks represent a versatile and efficient platform for quantitative bioprocesses. Their ability to maintain stable yet dynamic interactions enhance the precision and efficiency of biochemical processes. We demonstrated the directional transport of molecular cargoes from the satellites to their parent compartments by exploring molecular affinity. To show the potential of constructing synthetic cells, we performed life-like predator–prey interactions in the satellite–parent liposome networks by accomplishing enzymatic reactions. The satellite–parent liposome networks can be expanded to encompass many other multi-step chemical reaction pathways and more advanced life-like systems. Additionally, changes in the morphology of liposome networks, such as the detachment among liposomes, may provide insights into the remodelling of lipid bilayers during (synthetic) cell division. Compared to lipid-stabilized droplet networks,[45–47] our liposome networks are oil-free and more biocompatible to physiological environments, making them particularly useful for the exploration of quantitative bioprocesses, construction of life-like functional microsystems, and application in real-time biosensing.

Experimental

Microfluidics

Fluid components. To prepare monodisperse multi-core W/O/W double emulsion droplets (Fig. 1), aqueous solutions with 8% (w/v) polyethylene glycol (PEG, MW 6000 g mol^{-1}, VWR) and 2% (w/v) polyvinyl alcohol (PVA, MW 13 000–23 000 g mol^{-1}, 87–88% hydrolyzed, Sigma-Aldrich), a mixture of chloroform (Chl) and hexane (Hex)(36 : 64, v/v) containing 5 mg mL^{-1} 1,2-dioleoyl-sn-glycero-3-phosphocholine (DOPC, Avanti

Polar Lipids) as well as 10% (w/v) PVA with 1.5% (w/v) Pluronic F-68 (Sigma-Aldrich) were respectively utilized as inner water phase (W1), middle oil phase (O) and outer water phase (W2). 0.03% (w/v) Fluorescein isothiocyanate-dextran (FITC-Dextran, MW 40 000 g mol^{-1}, Sigma-Aldrich) and 0.03% (w/v) tetramethyl rhodamine-dextran (TRITC-Dextran, MW 40 000 g mol^{-1}, Sigma-Aldrich) were added in the W1 and W1′, respectively.

Microfluidic devices. Microfluidic devices used in this study are based on coaxial assemblies of round and square glass capillaries, as described in our previous publications.[12,13] In brief, the microfluidic devices consist of two stages (Fig. S1†). The first stage includes two or more flow-focusing drop generators. Here, two or more different types of W/O microdroplets were generated at the first stage, which were subsequently encapsulated at the second stage which consists of another flow-focusing drop generator with larger channels, forming W/O/W double emulsion droplets with multiple internal cores.

Manipulation. To generate the double emulsions with distinct multi-cores, all fluids were pumped into the capillary microfluidic devices using syringe pumps (LSP01-2A, Longer) at desired flow rates. Typical flow rates of the W1, W1′, O and W2 phases are 1000, 500, 800, and 3000 μL h^{-1}, respectively. The formation process of emulsion drops was monitored using an inverted optical microscope (Eclipse Ts2, Nikon) equipped with a high-speed camera (MicroC110, Phantom, Vision Research). Freshly prepared emulsions were collected in a semienclosed silicone isolation chamber (diameter 9 mm, height 0.12 mm, SecureSeal) covered with a glass coverslide for further characterization. The dewetting process and resultant labelled liposomes were observed using an optical microscope (IX71, Olympus) equipped with a high-speed camera (iXon Ultra 897 EMCCD, Andor) and a confocal laser scanning microscope (CLSM) (FV3000, Olympus).

Osmotic pressure-induced separation of satellite–parent liposome networks

The freshly prepared satellite–parent liposome networks were collected in semi-enclosed silicone isolation chambers (diameter 9 mm, height 0.12 mm, SecureSeal™) covered with a glass coverside. To induce separation of liposome networks, we added 150 mM NaCl to the sample at a rate of 5 μL h^{-1} for a total volume of 7 μL. The entire process was captured by a CLSM (FV3000, Olympus).

Transport of molecular cargoes between subcompartments of satellite–parent liposome networks

To achieve transport of fluorescent molecules from the satellite compartments (W1′) to the parent compartments (W1), the W1′, W1, O, and W2 phases were used as follows: W1′: an aqueous solution with 3% (w/v) PVA, 7% (w/v) PEG, 0.5 μM L^{-1} fluorescein (Sigma-Aldrich) and 2 μM melittin (Sigma-Aldrich); W1: an aqueous solution with 5% (w/v) PVA and 5% (w/v) PEG; O: a mixture of chloroform and hexane (36 : 64, v/v) containing 5 mg mL^{-1} DOPC; W2: an aqueous solution with 1% (w/v) PVA, 9% (w/v) PEG and 1.5% (w/v) Pluronic®F-68. The freshly

prepared liposome networks were collected in a closed silicone isolation chamber (diameter 9 mm, height 0.12 mm, Secure-Seal) covered with a glass coverslide, and then were captured at intervals of 0.5 min under a CLSM (FV3000, Olympus). Images were analyzed by ImageJ.

Micro-reaction stoichiometry in satellite–parent liposome networks

W1′: an aqueous solution with 3% (w/v) PVA, 7% (w/v) PEG, fluorescein diacetate (10 μg mL^{-1}, Sigma-Aldrich) in PBS buffer (pH 7.0). W1: an aqueous solution with 5% (w/v) PVA, 5% (w/v) PEG and 0.1 units per mL esterase (Shyuanye) in PBS buffer (pH 7.0). O: a mixture of chloroform and hexane (36 : 64, v/v) containing 5 mg mL^{-1} DOPC. W2: an aqueous solution with 1% (w/v) PVA, 9% (w/v) PEG and 1.5% (w/v) Pluronic®F-68 in PBS buffer (pH 7.0). The samples were collected and observed in the same manner as the transport of molecular cargoes between subcompartments of satellite–parent liposome networks. After the reaction was complete, we slowly added 150 mM NaCl into the samples to induce the satellite compartments to detach from the parent compartment. The processes were captured at intervals of 2 min under a CLSM (FV3000, Olympus).

Data availability

The data supporting this article have been included as part of the ESI.†

Author contributions

N. N. D. supervised the research. N. N. D. conceived the research and designed the experiments. J. Q. T. performed the experiments. J. Q. T. and N. N. D. wrote the paper. All authors approved the manuscript.

Conflicts of interest

There are no conflicts to declare.

Acknowledgements

References

1 J. W. Szostak, D. P. Bartel and P. L. Luisi, *Nature*, 2001, **409**, 387–390.

2 C. Xu, N. Martin, M. Li and S. Mann, *Nature*, 2022, **609**, 1029–1037.

3 N. A. Yewdall, A. F. Mason and J. C. Van Hest, *Interface Focus*, 2018, **8**, 20180023.

4 D. T. Hughes and V. Sperandio, *Nat. Rev. Microbiol.*, 2008, **6**, 111–120.

5 M. Archetti and K. J. Pienta, *Nat. Rev. Cancer*, 2019, **19**, 110–117.

6 H. Du, J. M. Bartleson, S. Butenko, V. Alonso, W. F. Liu, D. A. Winer and M. J. Butte, *Nat. Rev. Immunol.*, 2023, **23**, 174–188.

7 P. A. Beales and T. K. Vanderlick, *Adv. Colloid Interface Sci.*, 2014, **207**, 290–305.

8 I. Ivanov, S. K. Smoukov, E. Nourafkan, K. Landfester and P. Schwille, *Confl. Models. Orig. Life*, 2023, 303–326.

9 W. Mu, Z. Ji, M. Zhou, J. Wu, Y. Lin and Y. Qiao, *Sci. Adv.*, 2021, **7**, eabf9000.

10 E. Rideau, R. Dimova, P. Schwille, F. R. Wurm and K. Landfester, *Chem. Soc. Rev.*, 2018, **47**, 8572–8610.

11 N.-N. Deng, M. A. Vibhute, L. Zheng, H. Zhao, M. Yelleswarapu and W. T. S. Huck, *J. Am. Chem. Soc.*, 2018, **140**, 7399–7402.

12 N.-N. Deng, M. Yelleswarapu, L. Zheng and W. T. S. Huck, *J. Am. Chem. Soc.*, 2017, **139**, 587–590.

13 N.-N. Deng and W. T. S. Huck, *Angew. Chem., Int. Ed.*, 2017, **56**, 9736–9740.

14 Z.-H. Luo, C. Chen, Q.-H. Zhao and N.-N. Deng, *Sci. Adv.*, 2024, **10**, eadj4047.

15 N.-N. Deng, M. Yelleswarapu and W. T. Huck, *J. Am. Chem. Soc.*, 2016, **138**, 7584–7591.

16 J. M. Smith, D. Hartmann and M. J. Booth, *Nat. Chem. Biol.*, 2023, **19**, 1138–1146.

17 S. Berhanu, T. Ueda and Y. Kuruma, *Nat. Commun.*, 2019, **10**, 1325.

18 T. Furusato, F. Horie, H. T. Matsubayashi, K. Amikura, Y. Kuruma and T. Ueda, *ACS Synth. Biol.*, 2018, **7**, 953–961.

19 J.-Q. Tian, M.-Y. Chang, C. Chen, Z.-H. Luo, W. T. Huck and N.-N. Deng, *Nat. Chem. Eng.*, 2024, **1**, 450–461.

20 T. Litschel, B. Ramm, R. Maas, M. Heymann and P. Schwille, *Angew. Chem., Int. Ed.*, 2018, **57**, 16286–16290.

21 E. Godino, J. N. López, D. Foschepoth, C. Cleij, A. Doerr, C. F. Castellà and C. Danelon, *Nat. Commun.*, 2019, **10**, 4969.

22 M.-Y. Chang, H. Ariyama, W. T. Huck and N.-N. Deng, *Chem. Soc. Rev.*, 2023, **52**, 3307–3325.

23 N. De Franceschi, R. Barth, S. Meindlhumer, A. Fragasso and C. Dekker, *Nat. Nanotechnol.*, 2024, **19**, 70–76.

24 J. Zhao and X. Han, *Nat. Commun.*, 2024, **15**, 4956.

25 Y. Elani, R. V. Law and O. Ces, *Nat. Commun.*, 2014, **5**, 5305.

26 X. Wang, L. Tian, H. Du, M. Li, W. Mu, B. W. Drinkwater, X. Han and S. Mann, *Chem. Sci.*, 2019, **10**, 9446–9453.

27 A. Galanti, R. O. Moreno-Tortolero, R. Azad, S. Cross, S. Davis and P. Gobbo, *Adv. Mater.*, 2021, **33**, 2100340.

28 P. Gobbo, A. J. Patil, M. Li, R. Harniman, W. H. Briscoe and S. Mann, *Nat. Mater.*, 2018, **17**, 1145–1153.

29 K. Ramsay, J. Levy, P. Gobbo and K. S. Elvira, *Lab Chip*, 2021, **21**, 4574–4585.

30 Y. Qiao, M. Li, D. Qiu and S. Mann, *Angew. Chem.*, 2019, **131**, 17922–17927.

31 C. E. Hoskin, V. R. Schild, J. Vinals and H. Bayley, *Nat. Chem.*, 2022, **14**, 650–657.

32 C. Qi, X. Ma, J. Zhong, J. Fang, Y. Huang, X. Deng, T. Kong and Z. Liu, *ACS Nano*, 2023, **17**, 16787–16797.

33 X. Zhang, C. Li, F. Liu, W. Mu, Y. Ren, B. Yang and X. Han, *Nat. Commun.*, 2022, **13**, 2148.

34 Y. Zhang, J. Riexinger, X. Yang, E. Mikhailova, Y. Jin, L. Zhou and H. Bayley, *Nature*, 2023, **620**, 1001–1006.

35 M. J. Booth, V. R. Schild, A. D. Graham, S. N. Olof and H. Bayley, *Sci. Adv.*, 2016, **2**, e1600056.

36 L. Song, M. R. Hobaugh, C. Shustak, S. Cheley, H. Bayley and J. E. Gouaux, *Science*, 1996, **274**, 1859–1865.

37 A. Dupin and F. C. Simmel, *Nat. Chem.*, 2019, **11**, 32–39.

38 B. C. Buddingh', J. Elzinga and J. C. M. van Hest, *Nat. Commun.*, 2020, **11**, 1652.

39 J. G. Carlton, H. Jones and U. S. Eggert, *Nat. Rev. Mol. Cell Biol.*, 2020, **21**, 151–166.

40 S. SenGupta, C. A. Parent and J. E. Bear, *Nat. Rev. Mol. Cell Biol.*, 2021, **22**, 529–547.

41 W. O. Hancock, *Nat. Rev. Mol. Cell Biol.*, 2014, **15**, 615–628.

42 F. Jülicher and R. Lipowsky, *Phys. Rev. E.*, 1996, **53**, 2670.

43 J. Nas, *Phil. J. Health. Res. Dev.*, 2020, **24**, 9–19.

44 X. Du, Y. Li, Y.-L. Xia, S.-M. Ai, J. Liang, P. Sang, X.-L. Ji and S.-Q. Liu, *Int. J. Mol. Sci.*, 2016, **17**, 144.

45 Y. Elani, X. C. I. Solvas, J. B. Edel, R. V. Law and O. Ces, *Chem. Commun.*, 2016, **52**, 5961–5964.

46 D. K. Baxani, A. J. Morgan, W. D. Jamieson, C. J. Allender, D. A. Barrow and O. K. Castell, *Angew. Chem., Int. Ed.*, 2016, **55**, 14240–14245.

47 G. Villar, A. D. Graham and H. Bayley, *Science*, 2013, **340**, 48–52.